Article

QZ1 and QZ2: Rapid, Reversible Quinoline-Derivatized Fluoresceins for Sensing Biological Zn(II)

Elizabeth M. Nolan, Jacek Jaworski, Ken-Ichi Okamoto, Yasunori Hayashi, Morgan Sheng, and Stephen J. Lippard

J. Am. Chem. Soc., **2005**, 127 (48), 16812-16823• DOI: 10.1021/ja052184t • Publication Date (Web): 10 November 2005

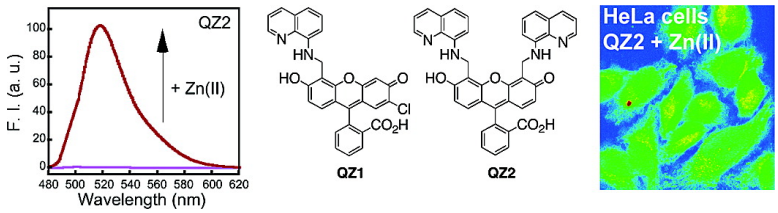

More About This Article

Additional resources and features associated with this article are available within the HTML version:

- Supporting Information
- Links to the 21 articles that cite this article, as of the time of this article download
- Access to high resolution figures
- Links to articles and content related to this article
- Copyright permission to reproduce figures and/or text from this article

View the Full Text HTML

J|A|C|S
ARTICLES
Published on Web 11/10/2005

QZ1 and QZ2: Rapid, Reversible Quinoline-Derivatized Fluoresceins for Sensing Biological Zn(II)

Elizabeth M. Nolan,[†] Jacek Jaworski,[‡,||,⊥] Ken-Ichi Okamoto,[‡,||,§] Yasunori Hayashi,[‡,||,§] Morgan Sheng,[‡,||,§,⊥] and Stephen J. Lippard*[,†]

Contribution from the Departments of Chemistry and Brain and Cognitive Sciences, Picower Institute for Learning and Memory, RIKEN-MIT Neuroscience Research Center, and Howard Hughes Medical Institute, Massachusetts Institute of Technology, Cambridge, Massachusetts 02139

Received April 5, 2005; E-mail: lippard@mit.edu

Abstract: QZ1, 2-[2-chloro-6-hydroxy-3-oxo-5-(quinolin-8-ylaminomethyl)-3*H*-xanthen-9-yl]benzoic acid, and QZ2, 2-[6-hydroxy-3-oxo-4,5-bis-(quinolin-8-ylaminomethyl)-3*H*-xanthen-9-yl]benzoic acid, two fluorescein-based dyes derivatized with 8-aminoquinoline, have been prepared and their photophysical, thermodynamic, and zinc-binding kinetic properties determined. Because of their low background fluorescence and highly emissive Zn(II) complexes, QZ1 and QZ2 have a large dynamic range, with ~42- and ~150-fold fluorescence enhancements upon Zn(II) coordination, respectively. These dyes have micromolar K_d values for Zn(II) and are selective for Zn(II) over biologically relevant concentrations of the alkali and alkaline earth metals. The Zn(II) complexes also fluoresce brightly in the presence of excess Mn(II), Fe(II), Co(II), Cd(II), and Hg(II), offering improved specificity for Zn(II) over di(2-picolyl)amine-based Zn(II) sensors. Stopped-flow kinetic investigations indicate that QZ1 and QZ2 bind Zn(II) with k_{on} values of $(3-4) \times 10^6$ M^{-1} s^{-1}, compared to $(6-8) \times 10^5$ M^{-1} s^{-1} for select ZP (Zinpyr) dyes, at 4.3 °C. Dissociation of Zn(II) from QZ1 and QZ2 occurs with k_{off} values of 150 and 160 s^{-1}, over 5 orders of magnitude larger than those for ZP probes, achieving reversibility on the biological (millisecond) time scale. Laser scanning confocal and two-photon microscopy studies reveal that QZ2 is cell-permeable and Zn(II)-responsive in vivo. Because of its weaker affinity for Zn(II), QZ2 responds to higher concentrations of intracellular Zn(II) than members of the ZP family, illustrating that binding affinity is an important parameter for Zn(II) detection in vivo.

Introduction

Zinc is an essential structural or catalytic component in over 300 metalloproteins,[1] is required for proper immune function,[2] is involved in DNA repair,[3] regulates caspase activity and apoptosis,[4] and is a proposed modulator of neurotransmission.[5] Although most zinc is tightly bound to proteins and its concentrations are strictly regulated by specific zinc transporters[6] and metallothionein,[7] pools of loosely bound and histochemically observable zinc exist in several tissues, including the pancreas[8] and brain.[5a,c] In the synaptic clefts of the mossy fiber region of the hippocampus, a region of the brain associated with learning and memory, concentrations of Zn(II) are reported to reach micromolar to submillimolar levels under normal physiological conditions.[9] This "free" zinc is housed in synaptic vesicles, presumably co-localized with glutamate, but its functional significance remains a mystery.[9,10] Pathologically, disruptions in zinc homeostasis have been associated with susceptibility to infectious diseases,[2] brain trauma and seizure,[11]

[†] Department of Chemistry.
[||] Department of Brain and Cognitive Sciences.
[‡] Picower Institute for Learning and Memory.
[§] RIKEN-MIT Neuroscience Research Center.
[⊥] Howard Hughes Medical Institute.

(1) Vallee, B. L.; Falchuk, K. H. *Physiol. Rev.* **1993**, *73*, 79−118.
(2) Walker, C. F.; Black, R. E. *Annu. Rev. Nutr.* **2004**, *24*, 255−275.
(3) (a) Daiyasu, H.; Osaka, K.; Ishino, Y.; Toh, H. *FEBS Lett.* **2001**, *503*, 1−6. (b) Ho, E.; Ames, B. N. *Proc. Natl. Acad. Sci. U.S.A.* **2002**, *99*, 16770−16775.
(4) (a) Truong-Tran, A. Q.; Carter, J.; Ruffin, R. E.; Zalewski, P. D. *Biometals* **2001**, *14*, 315−330. (b) Kimura, E.; Aoki, S.; Kikuta, E.; Koike, T. *Proc. Natl. Acad. Sci. U.S.A.* **2003**, *100*, 3731−3736.
(5) (a) Frederickson, C. J. *Int. Rev. Neurobiol.* **1989**, *31*, 145−238. (b) Huang, E. P. *Proc. Natl. Acad. Sci. U.S.A.* **1997**, *94*, 13386−13387. (c) Frederickson, C. J.; Bush, A. I. *Biometals* **2001**, *14*, 353−366. (d) Takeda, A. *Biometals* **2001**, *14*, 343−351. (e) Manzerra, P.; Behrens, M. M.; Canzoniero, L. M. T.; Wang, X. Q.; Heidinger, V.; Ichinose, T.; Yu, S. P.; Choi, D. W. *Proc. Natl. Acad. Sci. U.S.A.* **2001**, *98*, 11055−11061.
(6) (a) Liuzzi, J. P.; Cousins, R. J. *Annu. Rev. Nutr.* **2004**, *24*, 151−172. (b) Valente, T.; Auladell, C. *Mol. Cell. Neurosci.* **2002**, *21*, 189−204. (c) Cole, T. B.; Wenzel, H. J.; Kafer, K. E.; Schwartzkroin, P. A.; Palmiter, R. D. *Proc. Natl. Acad. Sci. U.S.A.* **1999**, *96*, 1716−1721. (d) Lee, J.-Y.; Cole, T. B.; Palmiter, R. D.; Koh, J.-Y. *J. Neurosci.* **2000**, *20*, RC79 1−5.
(7) (a) Jacob, C.; Maret, W.; Vallee, B. L. *Proc. Natl. Acad. Sci. U.S.A.* **1998**, *95*, 3489−3494. (b) Ebadi, M.; Iversen, P. L.; Hao, R.; Cerutis, D. R.; Rojas, P.; Happe, H. K.; Murrin, L. C.; Pfeiffer, R. F. *Neurochem. Int.* **1995**, *27*, 1−22. (c) Maret, W. *BioMetals* **2001**, *14*, 187−190. (d) Knipp, M.; Meloni, G.; Roschitzki, B.; Vašák, M. *Biochemistry* **2005**, *44*, 3159−3165.
(8) (a) Qian, W.-J.; Gee, K. R.; Kennedy, R. T. *Anal. Chem.* **2003**, *75*, 3468−3475. (b) Qian, W.-J.; Peters, J. L.; Dahlgren, G. M.; Gee, K. R.; Kennedy, R. T. *BioTechniques* **2004**, *37*, 922−933.
(9) (a) Vogt, K.; Mellor, J.; Tong, G.; Nicoll, R. *Neuron* **2000**, *26*, 187−196. (b) Howell, G. A.; Welch, M. G.; Frederickson, C. J. *Nature* **1984**, *308*, 736−738.
(10) (a) Kay, A. R. *J. Neurosci.* **2003**, *23*, 6847−6855. (b) Takeda, A. *Brain Res. Rev.* **2000**, *34*, 137−148. (c) Li, Y. V.; Hough, C. J.; Sarvey, J. M. *Science STKE* **2003**, 19. (d) Li, Y.; Hough, C. J.; Suh, S. W.; Sarvey, J. M.; Frederickson, C. J. *J. Neurophysiol.* **2001**, *86*, 2597−2604.
(11) (a) Choi, D. W.; Koh, J. Y. *Annu. Rev. Neurosci.* **1998**, *21*, 347−375. (b) Frederickson, C. J.; Maret, W.; Cuajungco, M. P. *The Neuroscientist* **2004**, *10*, 18−25.

10.1021/ja052184t CCC: $30.25

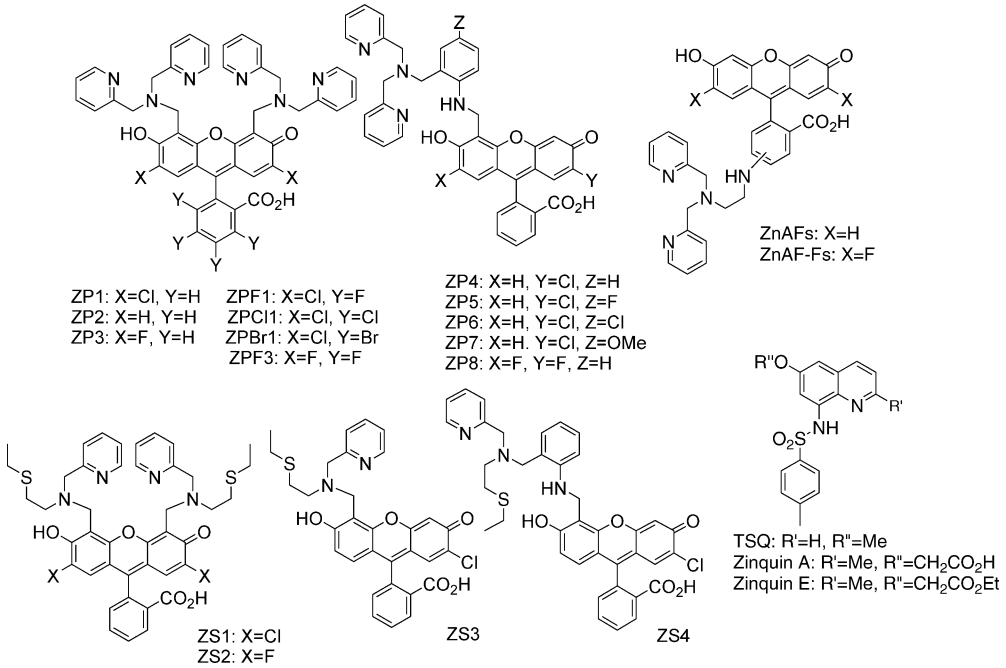

Figure 1. Selected fluorescent sensors for Zn(II). The ZP, ZS, and ZnAF dyes are all fluorescein-based and give fluorescence enhancement upon Zn(II) coordination. The quinoline sulfonamides, which include TSQ and Zinquin, are the most commonly used biological Zn(II) stains and also give fluorescence turn-on following Zn(II) binding.

and disorders that include depression,[12] diabetes,[13] prostrate cancer,[14] and several neurodegenerative states including Alzheimer's disease.[15]

To explore the trafficking of physiological and pathological zinc, much effort has been devoted to devising new tools and tactics for zinc detection.[16] Fluorescence imaging in particular is well-suited for live imaging of biological Zn(II), which has no facile spectroscopic or magnetic signature. Successful application of this methodology requires the development of robust Zn(II) imaging agents with high sensitivity, selectivity, and temporal fidelity. A variety of fluorescence-based approaches to Zn(II) detection have been documented recently, including small-molecule intensity-based[17] and ratiometric[18] sensors, as well as methods based on proteins[19] or peptides.[20] Although many of these systems are well-suited for investigating biological samples, arguably all suffer from one or more limitations, which continues to inspire the search for improved Zn(II) imaging tools.

The most widely used fluorescent histological Zn(II) stains, TSQ (*N*-(6-methoxy-8-quinolyl)-*p*-toluenesulfonamide) and its congeners (Figure 1), are quinoline derivatives bearing sulfonamide groups that give substantial fluorescence enhancement upon Zn(II) coordination.[21] Zinquin E, which harbors an ester moiety that hydrolyzes in vivo, is commonly employed because of its improved solubility, membrane permeability, and intracellular retention. These dyes require high-energy UV excitation (TSQ, $\lambda_{ex} = 334$ nm; Zinquin, $\lambda_{ex} = 370$ nm), however, which is potentially damaging to biological tissues and can induce autofluorescence from endogenous components. Despite a large dynamic range, these probes exhibit relatively dim emission deriving from a weakly fluorescent reporting group ($\Phi_{Zn} \approx 0.1$). For biological imaging applications, fluorescein is a superior

(12) García-Colunga, J.; Vázquez-Gómez, E.; Miledi, R. *Pharmacogenomics J.* **2004**, *4*, 388−393.
(13) Chausmer, A. B. *J. Am. Coll. Nutr.* **1998**, *17*, 109−115.
(14) Henshall, S. M.; et al. *Oncogene* **2003**, *22*, 6005−6012.
(15) (a) Cuajungco, M. P.; Lees, G. J. *Neurobiol. Dis.* **1997**, *4*, 137−169. (b) Bush, A. I. *Trends Neurosci.* **2003**, *26*, 207−214. (c) Bush, A. I. *Alzheimer Dis. Assoc. Disord.* **2003**, *17*, 147−150. (d) Suh, S. W.; Jensen, K. B.; Jensen, M. S.; Silva, D. S.; Kesslak, P. J.; Danscher, G.; Frederickson, C. J. *Brain Res.* **2000**, *852*, 274−278.
(16) (a) Kimura, E.; Koike, T. *Chem. Soc. Rev.* **1998**, *27*, 179−184. (b) Lim, N. C.; Freake, H. C.; Brückner, C. *Chem. Eur. J.* **2005**, *11*, 38−49. (c) Jiang, P.; Guo, Z. *Coord. Chem. Rev.* **2004**, *248*, 205−229. (d) Frederickson, C. *Science STKE* **2003**, 18. (e) Kikuchi, K.; Komatsu, K.; Nagano, T. *Curr. Opin. Chem. Biol.* **2004**, *8*, 182−191. (f) Burdette, S. C.; Lippard, S. J. *Proc. Natl. Acad. Sci. U.S.A.* **2003**, *100*, 3605−3610.
(17) (a) Canzoniero, L. M. T.; Sensi, S. L.; Choi, D. W. *Neurobiol. Dis.* **1997**, *4*, 275−279. (b) Kim, T. W.; Park, J.; Hong, J.-I. *J. Chem. Soc., Perkin Trans. 2* **2002**, 923−927. (c) Gee, K. R.; Zhou, Z.-L.; Qian, W.-J.; Kennedy, R. *J. Am. Chem. Soc.* **2002**, *124*, 776−778. (d) Sensi, S. L.; Ton-That, D.; Weiss, J. H.; Rothe, A.; Gee, K. R. *Cell Calcium* **2003**, *34*, 281−284. (e) Lim, N. C.; Yao, L.; Freake, H. C.; Brückner, C. *Bioorg. Med. Chem. Lett.* **2003**, *13*, 2251−2254. (f) Koike, T.; Watanabe, T.; Aoki, S.; Kimura, E.; Shiro, M. *J. Am. Chem. Soc.* **1996**, *118*, 12696−12703. (g) Kimura, E.; Ikeda, T.; Aoki, S.; Shionoya, M. *J. Inorg. Biol. Chem.* **1998**, *3*, 259−267. (h) Aoki, S.; Kaido, S.; Fujioka, H.; Kimura, E. *Inorg. Chem.* **2003**, *42*, 1023−1030. (i) Hirano, T.; Kikuchi, K.; Urano, Y.; Higuchi, T.; Nagano, T. *Angew. Chem., Int. Ed.* **2000**, *39*, 1052−1054. (j) Hirano, T.; Kikuchi, K.; Urano, Y.; Higuchi, T.; Nagano, T. *J. Am. Chem. Soc.* **2000**, *122*, 12399−12400. (k) Hirano, T.; Kikuchi, K.; Urano, Y.; Nagano, T. *J. Am. Chem. Soc.* **2002**, *124*, 6555−6562. (l) Czarnik, A. *Acc. Chem. Res.* **1994**, *27*, 302−308. (m) Wu, Y.; Peng, X.; Guo, B.; Fan, J.; Zhang, Z.; Wang, J.; Cui, A.; Gao, Y. *Org. Biomol. Chem.* **2005**, *5*, 1387−1392.
(18) (a) Maruyama, S.; Kikuchi, K.; Hirano, T.; Urano, Y.; Nagano, T. *J. Am. Chem. Soc.* **2002**, *124*, 10650−10651. (b) Henary, M. M.; Wu, Y.; Fahrni, C. J. *Chem. Eur. J.* **2004**, *10*, 3015−3025. (c) Taki, M.; Wolford, J. L.; O'Halloran, T. V. *J. Am. Chem. Soc.* **2004**, *126*, 712−713. (d) Lim, N. C.; Brückner, C. *Chem. Commun.* **2004**, 1094−1095. (e) Chang, C. J.; Jaworski, J.; Nolan, E. M.; Sheng, M.; Lippard, S. J. *Proc. Natl. Acad. Sci. U.S.A.* **2004**, *101*, 1129−1134. (f) Woodroofe, C. C.; Lippard, S. J. *J. Am. Chem. Soc.* **2003**, *125*, 11458−11459. (g) Woodroofe, C. C.; Won, A. C.; Lippard, S. J. *Inorg. Chem.* **2005**, *44*, 3112−3120. (h) Gee, K. R.; Zhou, Z.-L.; Ton-That, D.; Sensi, S. L.; Weiss, J. H. *Cell Calcium* **2002**, *31*, 245−251.
(19) (a) Elbaum, D.; Nair, S. K.; Patchan, M. W.; Thompson, R. B.; Christianson, D. W. *J. Am. Chem. Soc.* **1996**, *118*, 8381−8387. (b) Thompson, R. B.; Maliwal, B. P. *Anal. Chem.* **1998**, *70*, 1749−1754. (c) Thompson, R. B.; Whetsell, W. O.; Maliwal, B. P.; Fierke, C. A.; Frederickson, C. J. *J. Neurosci. Methods* **2000**, *96*, 35−45. (d) Fierke, C. A.; Thompson, R. B. *BioMetals* **2001**, *14*, 205−222. (e) Thompson, R. B.; Cramer, M. L.; Bozym, R.; Fierke, C. A. *J. Biomed. Opt.* **2002**, *7*, 555−560.
(20) (a) Stewart, J. D.; Roberts, V. A.; Crowder, M. W.; Getzoff, E. D.; Benkovic, S. J. *J. Am. Chem. Soc.* **1994**, *116*, 415−416. (b) Godwin, H. A.; Berg, J. M. *J. Am. Chem. Soc.* **1996**, *118*, 6514−6515. (c) Walkup, G. K.; Imperiali, B. *J. Am. Chem. Soc.* **1996**, *118*, 3053−3054. (d) Walkup, G. K.; Imperiali, B. *J. Am. Chem. Soc.* **1997**, *119*, 3443−3450. (e) Shults, M. D.; Pearce, D. A.; Imperiali, B. *J. Am. Chem. Soc.* **2003**, *125*, 10591−10597.

chromophore because of its high brightness ($\Phi \times \epsilon$; $\Phi \approx 1$, high ϵ), water solubility, desirable excitation (~480−500 nm) and emission (~520 nm) wavelengths, and the availability of suitable microscope equipment. Fluorescent Zn(II) sensors with one or two appended di(2-picolyl)amine (DPA) moieties as the receptor are especially valuable because they bind Zn(II) selectively over intracellular concentrations of Ca(II). DPA-derivatized, fluorescein-based zinc sensors include the ZnAF[17j,k] and ZP[22] families of dyes (Figure 1). Because the DPA fragment binds Zn(II) with a K_d of 70 nM,[23] DPA-appended sensors saturate at low Zn(II) concentrations. Moreover, Zn(II) coordination to DPA-derivatized dyes is irreversible on the millisecond time scale of many biological imaging experiments, as demonstrated by the present results and those in ref 17k, rendering them poorly suited for reporting time-dependent fluctuations in Zn(II) levels. Since DPA has a high affinity for other first-row transition metals ions, including Fe(II), Co(II), Ni(II), and Cu(II), Zn(II)-induced fluorescence can be compromised. Because of these shortcomings, the design of fluorescent Zn(II) chemosensors with alternative metal-coordinating moieties remains an important goal. In particular, it is of interest to install a more weakly zinc-binding unit, which conveys reversibility on the biological (millisecond) time scale, while retaining or improving selectivity for Zn(II). The ZS dyes (Figure 1) were developed in our laboratory as a first step toward this goal.[24] More recently, a series of ZnAF probes having modified pyridyl-based metal ion chelates that span a range of dissociation constants were reported.[25]

In the present article we describe new fluorescent Zn(II) chemosensors QZ1 and QZ2, fluorescein-based dyes containing one or two 8-aminoquinoline units on the xanthene moiety, that meet these criteria. QZ1 and QZ2 exhibit a number of advantageous photophysical, thermodynamic, and kinetic properties compared to TSQ and sensors that use DPA for Zn(II) binding. These features include (i) Zn(II)-specific fluorescence enhancement, (ii) improved selectivity for Zn(II) over other metal ions as compared to DPA sensors, (iii) micromolar dissociation constants, (iv) reversible Zn(II) binding, and (v) up to ~150-fold fluorescence enhancement upon Zn(II) coordination resulting from both low background fluorescence and highly emissive Zn(II) complexes.

(21) (a) Frederickson, C. J.; Kasarskis, E. J.; Ringo, D.; Frederickson, R. E. *J. Neurosci. Methods* **1987**, *20*, 91−103. (b) Zalewski, P. D.; Millard, S. H.; Forbes, I. J.; Kapaniris, O.; Slavotinek, A.; Betts, W. H.; Ward, A. D.; Lincoln, S. F.; Mahadevan, I. *J. Histochem. Cytochem.* **1994**, *42*, 877−884. (c) Kimber, M. C.; Mahadevan, I. B.; Lincoln, S. F.; Ward, A. D.; Tiekink, E. R. T. *J. Org. Chem.* **2000**, *65*, 8204−8209. (d) Nasir, M. S.; Fahrni, C. J.; Suhy, D. A.; Kolodsick, K. J.; Singer, C. P.; O'Halloran, T. V. *J. Biol. Inorg. Chem.* **1999**, *4*, 775−783. (e) Fahrni, C. J.; O'Halloran, T. V. *J. Am. Chem. Soc.* **1999**, *121*, 11448−11458. (f) Zalewski, P. D.; Forbes, I. J.; Seamark, R. F.; Borlinghaus, R.; Betts, W. H.; Lincoln, S. F.; Ward, A. D. *Chem. Biol.* **1993**, *1*, 153−161. (g) Zalewski, P. D.; Forbes, I. J.; Betts, W. H. *Biochem. J.* **1993**, *296*, 403−408. (h) Coyle, P.; Zalewski, P. D.; Philcox, J. C.; Forbes, I. J.; Ward, A. D.; Lincoln, S. F.; Mahadevan, I.; Rofe, A. M. *Biochem. J.* **1994**, *303*, 781−786.

(22) (a) Burdette, S. C.; Walkup, G. K.; Spingler, B.; Tsien, R. Y.; Lippard, S. J. *J. Am. Chem. Soc.* **2001**, *123*, 7831−7841. (b) Burdette, S. C.; Frederickson, C. J.; Bu, W.; Lippard, S. J. *J. Am. Chem. Soc.* **2003**, *125*, 1778−1787. (c) Nolan, E. M.; Burdette, S. C.; Harvey, J. H.; Hilderbrand, S. A.; Lippard, S. J. *Inorg. Chem.* **2004**, *43*, 2624−2635. (d) Chang, C. J.; Nolan, E. M.; Jaworski, J.; Burdette, S. C.; Sheng, M.; Lippard, S. J. *Chem. Biol.* **2004**, *11*, 203-210. (e) Chang, C. J.; Nolan, E. M.; Jaworski, J.; Okamoto, K.-I.; Hayashi, Y.; Sheng, M.; Lippard, S. J. *Inorg. Chem.* **2004**, *43*, 6774−6779. (f) Woodroofe, C. C.; Masalha, R.; Barnes, K. R.; Frederickson, C. J.; Lippard, S. J. *Chem. Biol.* **2004**, *11*, 1659−1666.

(23) Anderegg, G.; Hubmann, E.; Podder, N. G.; Wenk, F. *Helv. Chim. Acta* **1977**, *60*, 123−140.

(24) Nolan, E. M.; Lippard, S. J. *Inorg. Chem.* **2004**, *43*, 8310−8317.

(25) Komatsu, K.; Kikuchi, K.; Kojima, H.; Urano, Y.; Nagano, T. *J. Am. Chem. Soc.* **2005**, *127*, 10197−10204.

Experimental Section

Reagents. Ethyl acetate was dried over 3-Å molecular sieves. Anhydrous 1,2-dichloroethane (DCE) was purchased from Aldrich and used as received. The xanthene-functionalized fluorescein platforms, 7′-chloro-4′-fluoresceincarboxaldehyde[22c] (**1**) and 4′,5′-fluoresceindicarboxaldehyde[22a] (**2**), were synthesized as previously described. Sodium triacetoxyborohydride was purchased from Aldrich and 8-aminoquinoline from either Aldrich or Avacado.

Materials and Methods. Analytical thin-layer chromatography (TLC) was performed on Merck F254 silica gel plates (0.25 mm thickness) with UV light visualization. Whatman F254 silica gel-60 plates of 1 mm thickness were used for preparative TLC. NMR spectra were obtained on a Varian 300 or 500 MHz spectrophotometer operating at ambient probe temperature, 283 K, and both ^{1}H and ^{13}C NMR spectra were referenced to internal probe standards. IR spectra were obtained on an Avatar 360 FTIR instrument, and samples were prepared as KBr pellets. High-resolution mass spectrometry was conducted by staff at the MIT Department of Chemistry Instrumentation Facility.

2-[2-Chloro-6-hydroxy-3-oxo-5-(quinolin-8-ylaminomethyl)-3*H*-xanthen-9-yl]benzoic Acid (3, QZ1). To 5 mL of EtOAc were added 7′-chloro-4′-fluoresceincarboxaldehyde (**1**, 108 mg, 0.274 mmol) and 8-aminoquinoline (39 mg, 0.26 mmol). The reaction was stirred overnight at room temperature and an orange precipitate formed. The mixture was filtered and the precipitate was suspended in 10 mL of DCE. A portion (67 mg, 0.32 mmol) of $NaB(OAc)_3H$ was added and the reaction was stirred overnight at room temperature, during which time the solution clarified. The solvent was removed under reduced pressure and the crude material was purified by preparative TLC on silica gel (9:1 $CHCl_3$/MeOH), which afforded pure QZ1 as a magenta solid (53 mg, 38%): TLC $R_f = 0.48$ (silica, 9:1 $CHCl_3$/MeOH); mp > 325 °C (dec); ^{1}H NMR (CD_3OD, 300 MHz) δ 4.80 (2H, s), 6.65 (2H, m), 6.79 (1H, s), 6.92 (1H, s), 7.02 (1H, d), 7.13 (2H, m), 7.33 (2H, m), 7.62 (2H, m), 8.03 (2H, m), 8.61 (1H, m); ^{13}C NMR (DMF-d_7, 125 MHz) δ 49.10, 103.53, 105.07, 108.59, 110.01, 112.07, 112.94, 120.34, 121.74, 123.50, 126.49, 128.08, 128.15, 128.29, 128.58, 129.05, 129.73, 130.20, 130.94, 134.92, 136.08, 138.64, 141.07, 145.79, 146.98, 155.80, 156.96, 170.86, 173.43, 181.03; FTIR (KBr, cm^{-1}) 3416 (s, br), 1635 (m), 1578 (s), 1516 (m), 1455 (s), 1383 (s), 1340 (m), 1303 (m), 1225 (w), 1182 (w), 1153 (m), 1117 (w), 1087 (w), 1014 (m), 932 (w), 880 (w), 824 (w), 790 (w), 715 (w), 685 (w), 628 (w), 599 (w), 548 (w), 469 (w); HRMS (ESI) calcd MH$^+$ 523.1055, found 523.1061.

2-[6-Hydroxy-3-oxo-4,5-bis(quinolin-8-ylaminomethyl)-3*H*-xanthen-9-yl]benzoic Acid (4, QZ2). Portions of 8-aminoquinoline (74 mg, 0.51 mmol) and dialdehyde **2** (100 mg, 0.250 mmol) were combined in 3 mL of EtOAc and stirred overnight at room temperature. A light orange precipitate formed, the mixture was filtered, and the precipitate was washed with 3 mL of cold EtOAc. The precipitate was suspended in 4 mL of DCE, and $NaB(OAc)_3H$ (120 mg, 0.56 mmol) was added. The reaction became dark red and clarified over the course of ~2 h. The reaction was stirred for an additional 12 h and became orange. Preparative TLC of the reaction on silica gel (20:1 $CHCl_3$/MeOH) yielded pure QZ2 as a red-orange solid (47 mg, 29%): TLC $R_f = 0.47$ (silica, 9:1 $CHCl_3$/MeOH); mp > 325 °C (dec); ^{1}H NMR (CD_3OD, 300 MHz) δ 4.67 (4H, s), 6.57 (2H, s), 6.73 (2H, d), 6.92 (2H, d), 7.02 (2H, d), 7.11−7.16 (3H, m), 7.24−7.29 (2H, m), 7.51 (2H, m), 7.98 (3H, m), 8.52 (2H, d); ^{13}C NMR ($CDCl_3$, 125 MHz) δ 37.81, 107.12, 112.81, 113.75, 115.02, 122.33, 124.16, 129.16, 130.00, 130.15, 130.53, 131.16, 131.66, 134.93, 137.21, 139.83, 141.74, 146.48, 147.81, 158.16, 160.76, 174.66, 181.04; FTIR (KBr, cm^{-1}) 3046 (s, br), 3041 (w), 2950 (w), 2923 (w), 2846 (w), 1638 (m), 1579 (s), 1515 (s), 1442 (s), 1393 (s), 1378 (s), 1330 (s), 1231 (w), 1148 (m), 1095 (m), 1035 (w), 818 (m), 789 (m), 741 (w), 672 (w), 642 (w), 604 (w), 529 (w), 501 (w), 456 (m); HRMS (ESI) calcd MH$^+$ 645.2132, found 645.2132.

General Spectroscopic Methods. All aqueous solutions were prepared with Millipore water. Puratonic grade KCl was purchased from Calbiochem and molecular biology grade piperazine-*N*,*N*′-bis(2-ethanesulfonic acid) (PIPES) from Sigma. With the exception of the pK_a titrations, measurements were made at pH 7 in 50 mM PIPES, 100 mM KCl buffer. Excess ethylenediaminetetraacetic acid (EDTA) was added to solutions of apo QZ for quantum yield and extinction coefficient determination. Zinc stock solutions (100 mM, 500 mM) were prepared from anhydrous 99.999% $ZnCl_2$ and water. DMSO stock solutions (1 mM) of QZ1 and QZ2 were prepared, partitioned into ~300-μL aliquots, stored at −25 °C, and thawed in the dark before use. A gradual fluorescence rise is observed when solutions of QZ are allowed to stand for several hours at room temperature in the light. A starting solution of 10 mM KOH, 100 mM KCl, pH ~12, was used for pK_a titrations, and the pH of the solution was lowered by addition of 6, 2, 1, 0.5, or 0.1 N HCl. Quantum yields were measured using fluorescein in 0.1 N NaOH ($\Phi = 0.95$) as the standard.[26] Extinction coefficients were measured over a concentration range of 1−10 μM, except for the QZ2:Zn(II) complex, which was studied from 1 to 5 μM due to its limited solubility. Experimental details for all spectroscopic measurements performed in this study are available elsewhere.[22c] A Hitachi F-3010 spectrofluorimeter was used to record emission spectra. Optical absorption spectra were collected with a Cary 1E scanning spectrophotometer or a Hewlett-Packard 8453 diode array spectrophotometer. Circulating water baths were used to maintain all samples at 25 ± 1 °C. All spectroscopic measurements were repeated a minimum of three times and the resulting averages are reported.

Stopped-Flow Fluorescence Studies. Single-mixing stopped-flow kinetics studies were performed with a Hi-Tech SF-61 DX2 double-mixing stopped-flow apparatus equipped with a fluorescence detector. Excitation was provided at 505 (ZP1), 492 (ZP3), 495 (ZP4, QZ1), or 490 nm (QZ2). A GG495 glass cutoff filter (<455 nm) was placed over the exit to the photomultiplier tube, and emission was monitored from 455 to 700 nm. All solutions were prepared in 50 mM PIPES, 100 mM KCl, pH 7. Conditions for pseudo-first-order kinetics were maintained by using at least a 10-fold excess of Zn(II) in all experiments. With the exception of the temperature-dependent studies, all measurements were conducted at 4.3 ± 0.1 °C maintained by means of a circulating water bath. The temperature inside the sample chamber was monitored with an internal thermocouple.

Two series of concentration-dependent studies were performed. To determine the rate constants for Zn(II) binding to the selected ZP and QZ dyes, k_{on}, the concentration of Zn(II) was varied and multiple shots were taken at each Zn(II) concentration. To ensure that changes in dye concentration did not affect the observed rate constants and that dye aggregation did not occur, a series of experiments where the dye concentration was varied in the presence of at least 10-fold excess Zn(II) were also performed. Temperature-dependent studies were conducted to determine the activation enthalpy, $\Delta H^{\ddagger}$, and activation entropy, $\Delta S^{\ddagger}$, associated with Zn(II) coordination to ZP and QZ dyes. Values for k_{on} were determined in the presence of excess Zn(II) at a minimum of five temperatures over a range from ~4 to ~16 °C (QZ) or ~4 to ~40 °C (ZP). Each experiment was conducted a minimum of three times on different days and with different solutions, and the averages are reported. The observed rate constants obtained from all sets of experiments were calculated by employing the Kinet-Assyst software package (HiTech) to fit individual traces to monoexponentials and averaging the results for individual fits. Details for representative experiments are given as Supporting Information.

Cell Culture. HeLa cells were cultured in Dulbecco's Modified Eagle Medium (DMEM, Invitrogen) supplemented with 10% fetal calf serum (FCS, Invitrogen), glutamine (2 mM), penicillin (100 units/mL), and streptomycin (100 mg/mL). Two days before imaging, the cells were passed and plated on 10-mm glass coverslips. For labeling, cells were transferred to DMEM containing 1% FCS and incubated with 10 μM sensor at 37 °C under 5% CO_2. The cells were washed once with DMEM containing no FCS prior to imaging and/or zinc addition. Zinc was introduced to the cultured cells as the pyrithione salt using a Zn(II)/pyrithione ratio of 10:2. Stock solutions of $ZnCl_2$ (10−40 mM) and sodium pyrithione (20−80 mM) in DMSO were diluted 10-fold with DMEM prior to addition. In a typical experiment, a 100-μL aliquot of this solution was added to the cells bathed in 1 mL of DMEM. A stock solution of *N*,*N*,*N*′,*N*′-tetrakis(2-pyridylmethyl)ethylenediamine (TPEN, 10 or 20 mM) was also diluted 10-fold with DMEM containing no FCS prior to cell treatment. For experiments involving fixed cells, the cells were treated with 4% PFA (1 mL, PBS conaining 4% PFA and 4% surcose) for 5 min, washed 3 × 1 mL with PBS, and mounted onto glass microscope slides using the Vectashield antifading reagent (Vector Labs).

Laser Scanning Confocal Microscopy. A Zeiss LSM510 microscope equipped with a 63× objective (with 1.5× electronic zoom) was used to obtain confocal images. The samples were excited at 488 nm with an Ar laser. A *z*-series of seven slices taken at depth intervals of 0.75 nm was acquired for each image. The Metamorph software package was used for quantification.

Two-Photon Microscopy. Two-photon fluorescence imaging was conducted by using a custom-made two-photon laser scanning microscope based on an Olympus Fluoview 300/BX50WI microscope, equipped with a 60× objective lens and a 570-nm short-pass emission filter, and a Spectraphysics Tsunami Ti:sapphire laser pumped by Millennia Xs.

Results and Discussion

Design Considerations. Several factors were considered in the design of QZ1 and QZ2. Although a number of quinoline-containing fluorescent Zn(II) sensors exist,[21,27] none of these contain fluorescein as the reporting group. Given the superior photophysical properties of fluorescein and the successful application of quinoline derivatives in biological Zn(II) sensing, we expected a combination of quinoline and fluorescein to be advantageous. Since Zn(II) concentrations in the synaptic clefts of the hippocampus are presumed to reach near-millimolar concentrations, a Zn(II)-specific probe with a micromolar dissociation constant arguably should be useful to monitor Zn(II) flux in this region.[16d] The ZP dyes, although sensitive, bind Zn(II) irreversibly on the biological time scale (vide infra) and with sub-nanomolar dissociation constants, which prohibit their use for monitoring concentration changes in the micromolar to millimolar regime. Reducing the number of donor atoms in the coordination sphere is one way to raise the dissociation constant, which should be achieved by substitution of a N_3O or N_4O coordinating unit in the ZP sensor with a N_2O donor set. For controlling background fluorescence, a substantial body of work from our laboratory shows that aniline nitrogen atoms generally quench fluorescein emission more efficiently than tertiary amines.[22b,c,e] The ligand 8-aminoquinoline satisfies these additional criteria. We therefore installed 8-aminoquinoline moieties in the 4′- and 5′-positions of fluorescein to give N_2O donor sets with aniline-type nitrogen atoms that can act as photoinduced electron transfer (PET) switches.

Syntheses. Scheme 1 illustrates the syntheses of dyes QZ1 and QZ2 from 8-aminoquinoline and fluorescein aldehyde

(26) Brannon, J. H.; Madge, D. *J. Phys. Chem.* **1978**, *82*, 705−709.

(27) (a) Pearce, D. A.; Jotterand, N.; Carrico, I. S.; Imperiali, B. *J. Am. Chem. Soc.* **2001**, *123*, 5160−5161. (b) Xue, G.; Bradshaw, J. S.; Dalley, N. K.; Savage, P. B.; Izatt, R. M.; Prodi, L.; Montalti, M.; Zaccheroni, N. *Tetrahedron* **2002**, *58*, 4809−4815. (c) Mikata, Y.; Wakamatsu, M.; Yano, S. *Dalton Trans.* **2005**, 545−550.

Scheme 1

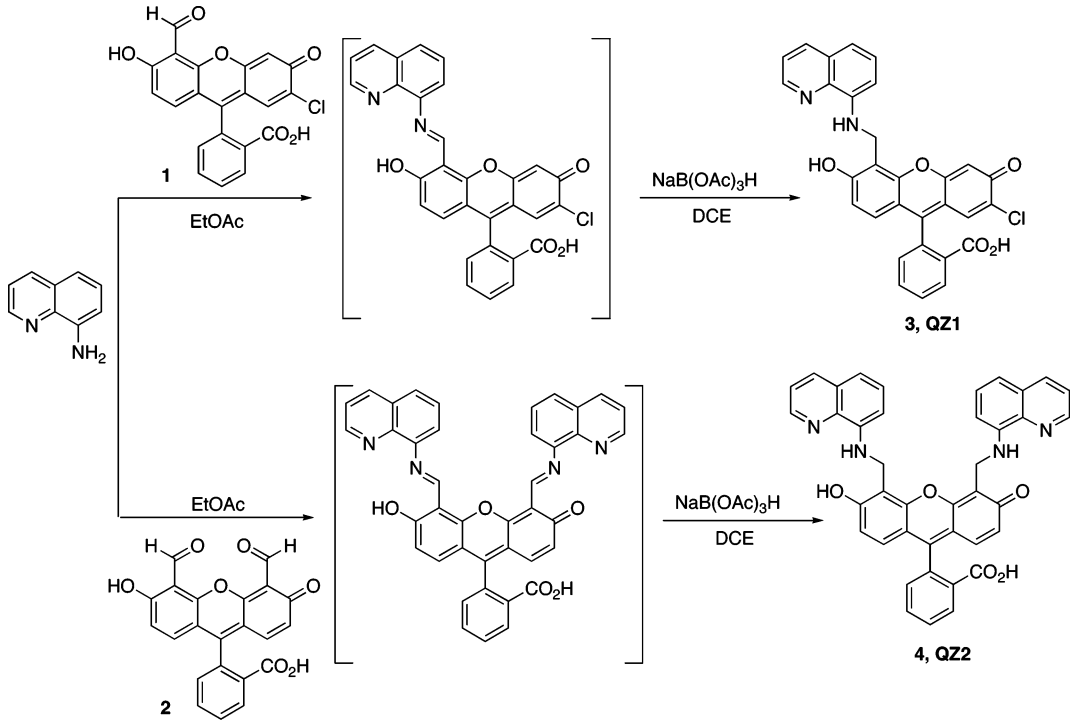

Table 1. Spectroscopic and Thermodynamic Data for Fluorescent Zn(II) Sensors[a]

	absorption λ (nm), $\epsilon \times 10^4$ (M^{-1} cm^{-1})		emission λ (nm), Φ[b]				
	unbound	Zn(II)	unbound	Zn(II)	pK_a[c] (N)	~DR[d]	ref
ZP1[e]	515, 7.9	507, 8.4	531, 0.38	527, 0.87	8.4	2.5	22a
ZP1(6-CO_2H)	516, 7.6	506, 8.1	531, 0.21	528, 0.63	7.1	7	22f
ZP2	498, 4.4	490, 5.3	522, 0.25	517, 0.92	9.4	4	22a
ZP3	502, 7.5	492, 8.5	521, 0.15	516, 0.92	6.8	6	22d
ZP4	506, 6.1	495, 6.7	521, 0.06	515, 0.34	7.2	4.4	22b,c
ZP5	504, 8.3	495, 9.1	520, 0.29	517, 0.48	9.6	1.6	22c
ZP6	506, 8.9	495, 9.8	519, 0.10	517, 0.34	6.3	4	22c
ZP7	505, 6.8	495, 7.7	521, 0.04	517, 0.05	6.9	1	22c
ZP8	500, 8.1	489, 7.8	516, 0.03	510, 0.35	6.5	11	22e
ZPF1	533, 9.9	525, 12.0	547, 0.11	544, 0.55	6.9	6	22d
ZPCl1	534, 9.7	527, 12.0	550, 0.22	549, 0.50	7.0	2.5	22d
ZPBr1	534, 4.5	528, 8.6	549, 0.25	547, 0.36	7.3	2.2	22d
ZPF3	520, 8.7	510, 9.3	537, 0.14	533, 0.60	6.7	5	22d
ZS1	510, 8.39	501, 7.52	531, 0.50	526, 0.70	7.7	1.4	24
ZS2	499, 6.69	489, 6.76	523, 0.39	516, 0.69	7.7	2	24
ZS3	500, 8.69		525, 0.71		9.3	1	24
ZS4	507, 8.11	495, ND	522, 0.12	520, 0.50	7.6	4.5	24
QZ1	505, 6.89	498, 6.98	524, 0.024	524, 0.78	6.1	42	this work
QZ2	499, 3.72	489 3.36	~520, 0.005	518, 0.70	7.0	150	this work

[a] All spectroscopic measurements were performed at pH 7 in 50 mM PIPES, 100 mM KCl buffer. [b] Fluorescein ($\Phi = 0.95$ in 0.1 N NaOH, ref 26) was used as the standard for quantum yield measurements. [c] Represents the pK_a value of the nitrogen atom responsible for PET switching in the probes. [d] DR is the dynamic range, or the ratio of integrated emission of the Zn-coordinated divided by the Zn-free fluorophore. [e] See Figure 1 for nomenclature. ZP1(6-CO_2H) has a carboxylate at the 6-position of the benzoate ring.

precursors, the latter of which were prepared in four or five steps according to previously described methodology.[22a,c] Condensation of 1 equiv of 8-aminoquinoline with monoaldehyde **1** in EtOAc resulted in precipitation of the intermediate imine as an orange solid. Reduction of the imine under mild conditions by using $NaB(OAc)_3H$ in DCE gave QZ1 in moderate yield following purification by preparative TLC on silica gel with $CHCl_3$/MeOH mixtures. QZ2 was obtained by an analogous procedure starting from the symmetrical dialdehyde **2** and 2 equiv of 8-aminoquinoline. Pure QZ1 and QZ2 are both magenta to red-orange solids that are readily soluble in MeOH. Through incorporation of a commercially available ligand moiety, the QZ syntheses are shorter and more economical than those for asymmetric ZP and ZS sensors, where multiple steps are required to assemble the ligand fragments.

Spectroscopic Properties of QZ1. Table 1 summarizes the results of fluorescence and UV−visible spectroscopic experiments conducted at pH 7 and 100 mM ionic strength (50 mM PIPES, 100 mM KCl) for QZ1 and QZ2. Selected results for the ZP and ZS sensors are included for comparison. Unbound QZ1, in the presence of excess EDTA to scavenge any potentially interfering metal ions, has a quantum yield of 0.024 ($\lambda_{max} = 524$ nm). Addition of excess Zn(II) causes the quantum yield to increase ~33-fold to 0.78 ($\lambda_{max} = 524$ nm). The

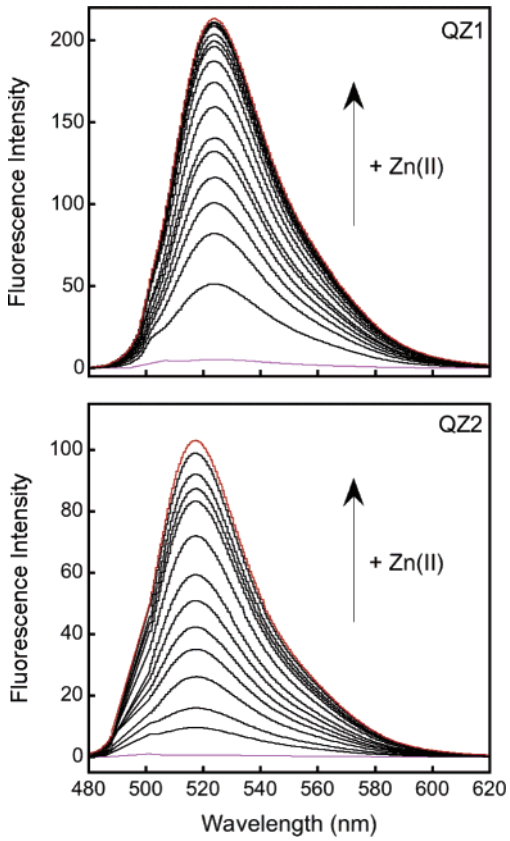

Figure 2. Fluorescence response of QZ1 and QZ2 to Zn(II) at pH 7 (50 mM PIPES, 100 mM KCl). Top: Emission of QZ1 before and after Zn(II) addition. Aliquots of 10 and 100 mM $ZnCl_2$ in water were added to yield Zn(II) concentrations of 0, 10, 20, 30, 40, 50, 60, 93, 127, 193, 260, 327, 392, 460, 526, 593, 760, and 927 μM. [QZ1] = 1 μM; λ_{ex} = 500 nm. Bottom: Emission of QZ2 before and after Zn(II) addition. Aliquots of 100 and 500 mM $ZnCl_2$ were added to yield Zn(II) concentrations of 0, 0.05, 0.1. 0.2, 0.35, 0.5, 0.7, 1.0, 1.5, 2.0, 2.75, 3.75, 4.75, and 6.75 mM. [QZ2] = 1 μM; λ_{ex} = 490 nm.

absorption spectrum undergoes a blue-shift from 505 nm (ϵ = 68 900 M^{-1} cm^{-1}) to 498 nm (ϵ = 69 800 M^{-1} cm^{-1}) upon Zn(II) binding, indicating a perturbation of the fluorescein π system by presumed Zn(II) coordination to the phenol. Taken together, there is a ~42-fold increase in integrated emission resulting from Zn(II) binding to QZ1 (Figure 2).

The pH dependence of the QZ1 fluorescence was investigated as shown in Figure 3. QZ1 fluorescence exhibits little change from pH ~12 to ~7 and reaches its maximum at pH ~5.5. Two protonation events affect QZ1 fluorescence, with pK_{a1} = 6.1 and pK_{a2} = 5.0. The former is assigned to the aniline nitrogen atom, and the latter value corresponds to protonation of the fluorescein and formation of a nonfluorescent state. Less than 2-fold fluorescence change occurs upon protonation of the aniline nitrogen atom compared to ~42-fold fluorescence enhancement upon Zn(II) coordination, rendering QZ1 relatively insensitive to pH changes.

Spectroscopic Properties of QZ2. QZ2, depicted in Scheme 1, is a symmetrical analogue of QZ1 and contains two 8-aminoquinoline moieties. We elected to prepare and characterize QZ2 on the basis of experience with several asymmetric and symmetric Zn(II) sensors previously synthesized in our laboratory. A comparison of the ZS1/ZS3 couple (Figure 1) shows that installation of a second tertiary amine-based ligand on the xanthene framework results in a substantial decrease in

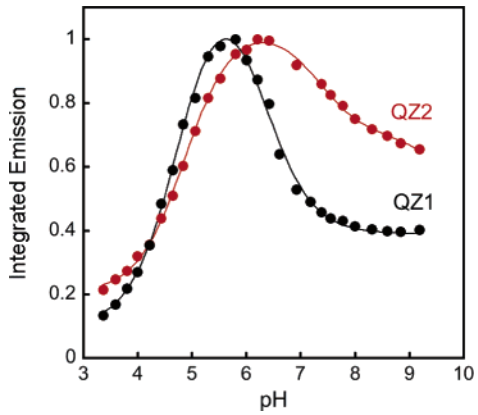

Figure 3. Fluorescence dependence on pH for QZ1 (black) and QZ2 (red). Solutions of 1 μM QZ were prepared in 10 mM KOH, 100 mM KCl, pH ~12, and the emission spectra recorded. The pH was decreased in increments of ~0.25 by addition of 6, 2, 1, 0.5, and 0.1 N HCl, and the emission spectra were recorded at each point. The emission was integrated, normalized, and plotted against pH. Excitation was provided at 495 nm. Points above pH ~10 are omitted from the plot since no significant emission changes occurred.

background fluorescence (symmetric ZS1 Φ_{free} = 0.50; asymmetric ZS3 Φ_{free} = 0.71).[24] A similar trend occurs for DPA-based ZP1 and its asymmetric analogue.[28] Such "cooperative quenching" has recently been documented in *N*-arylpiperazine-substituted 2′,7′-dichlorofluoresceins.[29] This behavior makes intuitive sense when the simple PET quenching mechanism is considered.[30] According to this model, a free nitrogen lone pair quenches the metal-free dyes by electron transfer into the hole produced during photoexcitation. Given that symmetrical sensors have two nitrogen lone pairs available to quench the fluorophore excited state, compared to only one nitrogen lone pair in the asymmetrical analogues, relatively less background fluorescence is expected. We reasoned that a symmetric QZ dye would exhibit even further reduced background fluorescence than asymmetrical QZ1 while maintaining the high degree of Zn(II)-induced turn-on exhibited by QZ1.

In accord with this expectation, apo QZ2 has a very low quantum yield of 0.005 ($\lambda_{max} \approx$ 520 nm) at pH 7 (50 mM PIPES, 100 mM KCl) and in the presence of EDTA to complex any potentially interfering metal ions (Table 1). An ~150-fold fluorescence increase occurs upon introduction of excess Zn(II) to a solution of QZ2 (Figure 2), and the quantum yield for the Zn(II)-bound complex is 0.70 (λ_{max} = 518 nm). The absorption spectrum of QZ2 blue-shifts by 10 nm upon Zn(II) coordination, moving from 499 nm (ϵ = 37 200 M^{-1} cm^{-1}) to 489 nm (ϵ = 33 600 M^{-1} cm^{-1}). This blue-shift reflects a perturbation of the fluorescein π system and is consistent with the phenol oxygen atom being involved in Zn(II) binding. The relatively low extinction coefficients of QZ2 are reminiscent of those determined for the fluorescein-based, DPA-derivatized Zn(II) sensor ZP2 (Table 1) and can be rationalized on the basis of the nature of the fluorescein chromophore. Unsubstituted fluorescein has an extinction coefficient of ~77 000 M^{-1} cm^{-1} (0.1 N NaOH),[31] and fluoresceins halogenated in the 2′- and 7′-positions exhibit

(28) Chang, C. J.; Nolan, E. M.; Lippard, S. J. Unpublished results.
(29) Sparano, B. A.; Shahi, S. P.; Koide, K. *Org. Lett.* **2004**, *6*, 1947−1949.
(30) (a) de Silva, A. P.; Gunaratne, H. Q. N.; Gunnlaugsson, T.; Huxley, A. J. M.; McCoy, C. P.; Rademacher, J. T.; Rice, T. E. *Chem. Rev.* **1997**, *97*, 1515−1566. (b) de Silva, A. P.; Fox, D. B.; Huxley, A. J. M.; Moody, T. S. *Coord. Chem. Rev.* **2000**, *205*, 41−57.
(31) Sjöback, R.; Nygren, J.; Kubista, M. *Spectrochim. Acta, Part A* **1995**, *51*, L7−L21.

more intense absorption. For instance, the reported extinction coefficient for 2′,7′-dichlorofluorescein is 101 000 M^{-1} cm^{-1} (0.1 N NaOH).[32] Relative extinction coefficients for our dyes with and without chloro substitution in these positions (ZP1/ZP2, QZ1/QZ2) reflect this trend.

Figure 3 includes a representative pK_a titration of QZ2, which shows that two protonation events influence QZ2 emission. The pK_a values of 7.0 and 4.9 are assigned to aniline nitrogen and fluorescein protonation, respectively. Only ~2-fold fluorescence enhancement occurs upon protonation of the aniline nitrogen atom, compared to the ~150-fold fluorescence increase associated with Zn(II) coordination, which indicates that QZ2 fluorescence is also virtually insensitive to protons. This feature is an improvement over symmetric sensors ZP1−3, which display greater degrees of proton-induced fluorescence turn-on. It is also relevant to biological imaging studies, where changes in proton concentration may occur and potentially interfere with the Zn(II) response of a proton-sensitive dye.

Metal-Binding Properties of QZ1 and QZ2. The acquisition of molecules with varying dissociation constants (K_d) is an important goal in biological Zn(II) sensor development. Since near-millimolar concentrations of Zn(II) are presumed to exist in synaptic clefts located in substructures of the mammalian hippocampus, fluorescent Zn(II) sensors with K_d values in the mid- to high-micromolar range will be advantageous for imaging this pool. Investigations of Zn(II) pathology involving high influx levels of Zn(II) could also benefit from such low-affinity chemosensors. In contrast to the ZP sensor family, members of which bind Zn(II) with subnanomolar affinity, QZ1 and QZ2 exhibit maximum fluorescence response in the presence of high-micromolar to millimolar concentrations of Zn(II). Metal binding titrations monitored by fluorescence spectroscopy revealed that QZ1 gives maximum emission in the presence of ~300 μM Zn(II), with an apparent K_d value of 33 ± 2 μM at 25 °C (Figure 2 and Figure S1, Supporting Information). A similar value, 48 ± 3 μM, was obtained from stopped-flow kinetic studies performed at 4.3 °C (see below). Sensor QZ2 can coordinate two Zn(II) ions and responds to even higher concentrations of Zn(II). Fluorescence titrations reveal that ~50% of the total fluorescence increase occurs when QZ2 encounters ~770 μM Zn(II), and low-millimolar concentrations are required to achieve full fluorescence enhancement (Figure 2 and Figure S1). Stopped-flow kinetic experiments (see Figure 6 and discussion below) indicate a K_{d1} value of 41 ± 3 μM for Zn(II) binding to QZ2 at 4.3 °C, comparable to that of QZ1. As anticipated from the micromolar affinity of each QZ dye for Zn(II), the metal ion binding events are readily reversible. Addition of the heavy metal chelator TPEN to solutions of QZ and Zn(II) decreases the fluorescence to baseline immediately upon mixing (Figure S2).

The coordination of QZ1 and QZ2 to Zn(II) was also explored by using UV−visible spectroscopy. The absorption spectra of both dyes are dominated by the fluorescein chromophore, as anticipated, and slight (~10 nm) blue-shifts in absorption occur upon Zn(II) binding. The resulting difference spectra for the QZ dyes are comparable to those obtained for members of the ZP family and presumably reflect a similar perturbation to the fluorescein π system resulting from Zn(II) coordination, attributed to phenol coordination.[22a] For QZ1, Zn(II) coordination results in an absorption increase at 492 nm and decreases at 513 and 250 nm (Figure 4). Less prominent features are observed at 460, 317, and 283 nm. The difference spectrum for QZ2 has analogous features, with an absorption increase at 482 nm and a decrease at 504 nm.

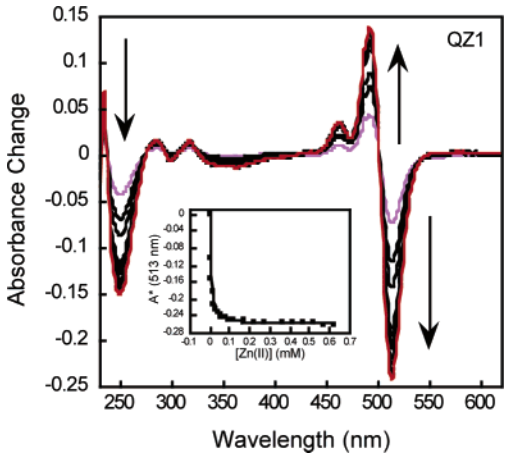

Figure 4. Optical absorption difference spectra for the addition of Zn(II) to QZ1 at pH 7 (50 mM PIPES, 100 mM KCl). Decreases in absorption are observed at 513 and 250 nm, whereas absorption increases occur at 492, 462, 317, and 283 nm. Inset: The absorption change at 513 nm plotted against the concentration of Zn(II) in solution. The absorption due to the free dye was subtracted from all data. [QZ1] = 5 μM.

QZ1 was designed to bind Zn(II) with 1:1 stoichiometry. Fluorescence spectroscopy was employed to verify the solution stoichiometry of the QZ1:Zn(II) complex. Job plot analyses revealed a break at 0.5, indicating formation of a 1:1 species in solution (Figure S3). This feature may be beneficial for calibration purposes in vivo. Since Zn(II) forms four-, five-, and six-coordinate complexes, we propose that one or more water molecules or buffer components complete the Zn(II) coordination sphere defined by the N_2O donor set of the QZ ligand system. Given the two 8-aminoquinoline moieties, QZ2 can bind one or two Zn(II) ions, depending on the concentration of Zn(II) in solution. The second Zn(II)-binding event is of significantly lower affinity, because millimolar Zn(II) is required for saturation (Figure 2 and Figure S1); its K_d value was not determined.

Zn(II) Selectivity of QZ1 and QZ2. One challenge in Zn(II) sensor development is to procure systems that are selective for Zn(II) over a wide range of potentially competing metal ions. DPA is a valuable ligand for biological Zn(II) sensing because of its high affinity for Zn(II) over Ca(II), but dyes containing this ligand moiety readily bind other divalent metal ions that block Zn(II) coordination. Fluorescence spectroscopy was employed to investigate the selectivity of QZ1 and QZ2 for Zn(II) over biologically relevant alkali and alkaline earth metals, divalent first-row transition metals, Cd(II), and Hg(II); representative data for QZ2 are shown in Figure 5 (see Figure S3 for QZ1 data). QZ1 and QZ2 readily detect Zn(II) in the presence of millimolar concentrations of Na(I), K(I), Ca(II), and Mg(II), indicating that these physiologically relevant components will not interfere with QZ detection of Zn(II) in such samples. Of the first-row transition metals considered, only Ni(II) and Cu(II) compromise the Zn(II)-induced fluorescence enhancement of the QZ sensors. This selectivity is a substantial advantage over ZP1−8, which preferentially bind Fe(II) and

(32) Leonhardt, H.; Gordon, L.; Livingston, R. *J. Phys. Chem.* **1971**, *75*, 245−249.

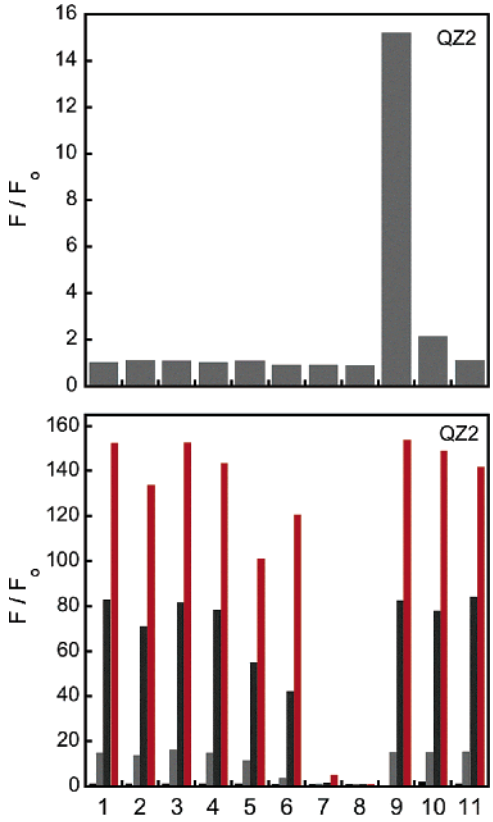

Figure 5. Selectivity of QZ2 for Zn(II). Top: Fluorescence response of QZ2 following addition of 50 equiv of the metal ion of interest: **1**, Na(I); **2**, Ca(II); **3**, Mg(II); **4**, Mn(II); **5**, Fe(II); **6**, Co(II); **7**, Ni(II); **8**, Cu(II); **9**, Zn(II); **10**, Cd(II); **11**, Hg(II). Bottom: Selectivity of QZ2 for Zn(II) over the metal ions of interest. Black bars: QZ2 + 50 equiv cation, as shown in the top panel. Light gray bars: addition of 50 equiv of Zn(II) to the solution containing QZ2 and the cation of interest. Dark gray bars: introduction of an additional 450 equiv of Zn(II) to the solution containing QZ2 and the cation of interest. Red bars: introduction of an additional 2000 equiv of Zn(II). Samples were excited at 495 nm, and the emission spectra were integrated from 510 to 650 nm. All data (F) are normalized with respect to the emission of the free dye (F_o). [QZ2] = 1 μM. QZ1 data are given as Supporting Information (Figure S4).

Co(II) in addition to Ni(II) and Cu(II). The QZ chemosensors also differentiate Zn(II) from Cd(II). Complexation to Cd(II) results in only negligible fluoresence enhancement, and Zn(II) readily displaces Cd(II) from the metal ion coordination sphere. This behavior contrasts with that of the ZP and ZS dyes, which show comparable turn-on for both Zn(II) and Cd(II).[22c,24]

Kinetic Investigations of ZP and QZ Sensors. The fluorescence response of the ZP and QZ dyes to zinc can be observed by the eye or with a hand-held UV lamp to occur immediately upon mixing. Stopped-flow fluorescence studies were therefore conducted to measure the rate constants for Zn(II) association, via fluorescence turn-on, for QZ1, QZ2, and several representative ZP dyes. Rate constants for Zn(II) dissociation were either measured (QZ) or calculated (ZP) from k_{on} and experimentally determined dissociation constants. Equations 1 and 2 illustrate the relationship between the dissociation constant, K_d, the rate constants for Zn(II) binding, k_{on}, and Zn(II) release, k_{off}, and the observed pseudo-first-order rate constant, k_{obs}. To verify that k_{obs} is independent of initial dye concentration, a series of experiments were conducted where the dye concentration (after mixing) was varied from 0.5 to 5 μM in the presence of at least 10-fold excess Zn(II); the results are detailed in the Supporting Information. For each dye, this experiment showed that k_{obs} is independent of initial dye concentration, which confirmed that dye aggregation or other potentially interfering phenomena were not occurring during the course of the experiment.

$$k_{obs} = k_{on}[\mathrm{Zn(II)}] + k_{off} \quad (1)$$

$$K_d = k_{off}/k_{on} \quad (2)$$

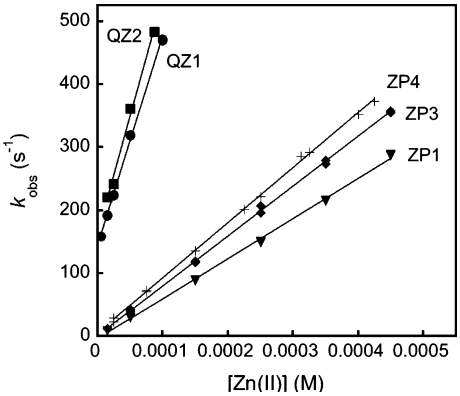

Figure 6. Results from stopped-flow fluorescence studies of Zn(II) binding to various Zn(II) sensors. Plots of k_{obs} vs concentration of Zn(II) for QZ1 (●), QZ2 (■), ZP1 (▲), ZP3 (◆), and ZP4 (+). All data were collected at 4.3 ± 0.1 °C. See the Supporting Information for kinetic traces, monoexponential fits, individual plots, and experimental details.

Given the subnanomolar dissociation constants of the ZP dyes, essentially no back-reaction is observed on the time scale of the stopped-flow measurements, and eq 1 can be simplified to eq 3. Plots of k_{obs} vs Zn(II) concentration for Zn(II) binding to

$$k_{obs} = k_{on}[\mathrm{Zn(II)}] \quad (3)$$

the selected ZP dyes illustrate this notion since the lines pass through the origin (Figure 6). The data in Table 2 show that ZP dyes are characterized by k_{on} values in the range of (6.3−8.5) × 10^5 M^{-1} s^{-1} at 4.3 °C. Kinetic data from temperature-dependent studies (see Figure 8 and discussion below) afford k_{on} values of (3.3−5.2) × 10^6 M^{-1} s^{-1} at 25 °C for the ZP sensors. These association constants indicate that the ZP dyes can respond to Zn(II) on the millisecond time scale and are similar to those obtained for the ZnAF dyes ((3.1−4.3) × 10^6 M^{-1} s^{-1} at 25 °C), which also utilize DPA as the Zn(II) chelate.[17k] Association rates for fluorescent macrocycle-based Zn(II) sensors are notably slower, generally exhibiting k_{on} values of 10−10^2 M^{-1} s^{-1},[17h] due to the rigidity of the ligand moiety.[17e,h] Members of the ZP family display rapid Zn(II) complexation and, as calculated from the K_d and k_{on} values, relatively slow Zn(II) dissociation. The latter feature will be prohibitive for many imaging applications. Equation 2 affords k_{off} values in the range of (2.3−3.4) × 10^{-3} s^{-1} at 25 °C and yield $t_{1/2}$ = 200−300 s for Zn(II) dissociation from ZP.

In contrast, the QZ dyes display readily reversible Zn(II) coordination. The kinetic data for QZ1 and QZ2 depicted in Figure 6 yield k_{on} values of (3.1−3.9) × 10^6 M^{-1} s^{-1} at 4.3 °C, indicating faster Zn(II) complexation as compared to ZP, and return k_{off} values of 150 and 160 s^{-1}, respectively, at this temperature. Given the fast association rates observed for QZ, we were unable to obtain reliable kinetic data above 16 °C. Extrapolation of the Eyring plots in Figure 7 yields estimated k_{on} values of 3.7 × 10^7 and 4.5 × 10^7 M^{-1} s^{-1} and k_{off} values

Table 2. Kinetic and Thermodynamic Parameters for Zn(II) Binding to ZP and QZ Sensors[a]

	k_{on} (M^{-1} s^{-1})		K_{d1}		k_{off} (s^{-1})			
	4.3 °C[b]	25 °C[c]	4.3 °C[d]	25 °C[e]	4.3 °C[f]	25 °C[g]	$\Delta H^{\ddagger}$ [h] (kcal/mol)	$\Delta S^{\ddagger}$ [h] (cal/mol·K)
ZP1	$(6.3 \pm 0.1) \times 10^5$	$(3.3 \pm 0.4) \times 10^6$		0.7 ± 0.1 nM		$(2.3 \pm 0.4) \times 10^{-3}$	12.5 ± 0.1	13.2 ± 0.3
ZP3	$(7.8 \pm 0.1) \times 10^5$	$(4.3 \pm 0.3) \times 10^6$		0.7 ± 0.1 nM		$(2.9 \pm 0.4) \times 10^{-3}$	11.6 ± 0.2	10.7 ± 0.7
ZP4	$(8.5 \pm 0.4) \times 10^5$	$(5.2 \pm 0.1) \times 10^6$		0.65 ± 0.1 nM		$(3.4 \pm 0.5) \times 10^{-3}$	12.2 ± 0.3	13.1 ± 0.1
QZ1	$(3.1 \pm 0.2) \times 10^6$	$(3.7 \pm 0.2) \times 10^7$	$48 \pm 3\ \mu$M	$33 \pm 2\ \mu$M	$(1.5 \pm 0.3) \times 10^2$	$(1.2 \pm 0.1) \times 10^3$	10.7 ± 0.1	12.1 ± 0.1
QZ2	$(3.9 \pm 0.3) \times 10^6$	$(4.5 \pm 0.3) \times 10^7$	$41 \pm 3\ \mu$M		$(1.6 \pm 0.2) \times 10^2$		10.7 ± 0.1	12.4 ± 0.1

[a] All measurements were made at pH 7 (50 mM PIPES, 100 mM KCl). [b] Experimentally determined values for k_{on} at 4.3 ± 0.1 °C. [c] Experimentally determined k_{on} for ZP sensors at 25 ± 0.1 °C. The k_{on} values for QZ were estimated by extrapolation of the Eyring plots (Figure 7). [d] Dissociation constants for QZ1 and QZ2 calculated from stopped-flow kinetic data obtained at 4.3 ± 0.1 °C. [e] Dissociation constants for ZP and QZ1 obtained experimentally by fluorimetric titration at 25 ± 1 °C. ZP data were taken from refs 22a,b,d. [f] Experimentally determined k_{off} at 4.3 ± 0.1 °C. [g] Calculated k_{off} for ZP at 25 ± 1 °C. [h] Activation parameters were determined over a temperature range from ~4 to ~20 °C for QZ and from ~4 to ~40 °C for ZP.

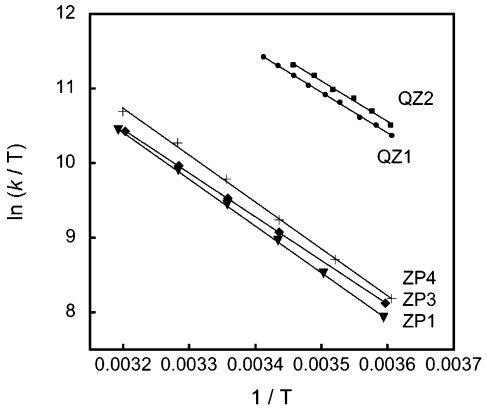

Figure 7. Eyring plots for QZ1 (●), QZ2 (■), ZP1 (▲), ZP3 (◆), and ZP4 (+). The temperature was varied from ~4 to ~16 °C (QZ) or from ~4 to ~40 °C (ZP). Calculated values for $\Delta H^{\ddagger}$ and $\Delta S^{\ddagger}$ are given in Table 2.

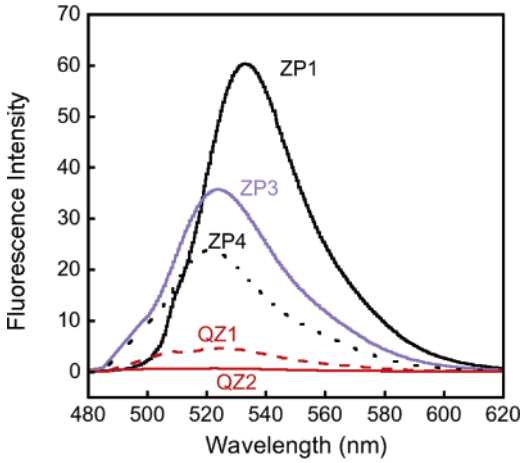

Figure 8. Relative fluorescence emission of 1 μM ZP1, ZP3, ZP4, QZ1, and QZ2. Solutions were prepared at pH 7 with 50 mM PIPES, 100 mM KCl, pH 7, with excess EDTA.

of $>10^3$ s^{-1} for QZ1 and QZ2 at 25 °C. These computed k_{off} values are over 5 orders of magnitude greater than those observed for the ZP and ZnAF systems and yield $t_{1/2} < 0.5$ ms. The QZ dissociation rates are greater than those of Fura-2, Indo-1, and Quin-2, fluorescent Ca(II) sensors that have been successfully used to measure Ca(II) changes in biological specimens.[33] This feature makes the QZ dyes potentially useful for biological studies that involve monitoring Zn(II) flux, such as those proposed to occur at synapses.

The fast association rates for Zn(II) complexation to QZ1 and QZ2 necessitated low-temperature stopped-flow investigations. To ascertain the effect of temperature on the association rate, a series of temperature variation experiments were conducted and are detailed in the Supporting Information. Figure 7 illustrates the Eyring plots for the ZP and QZ dyes under study. Values for the activation enthalpy, $\Delta H^{\ddagger}$, and activation entropy, $\Delta S^{\ddagger}$, associated with Zn(II) binding are given in Table 2. The ZP and QZ dyes all have $\Delta H^{\ddagger}$ between 10.7 and 12.5 kcal/mol, which reflects a relatively low activation barrier and fast rate of association. Values for $\Delta S^{\ddagger}$ are positive and range from 10.7 to 13.2 cal/mol·K. The positive $\Delta S^{\ddagger}$ values may be due to dissociation of buffer components from the reacting species in the transition state.

Comparison of QZ to ZP and Other Fluorescent Zn(II) Sensors. A comparison of spectroscopic and photophysical features of the QZ vs the ZP and ZS dyes reveals some expected similarities and several striking differences (Table 1). With the exception of ZP5, the asymmetrical aniline-derivatized ZP dyes, ZP4−8, have $\Phi_{free} < 0.1$, the latter of which is attributed to PET quenching of the fluorescein excited state at physiological pH by the aniline nitrogen lone pair.[22c] The quantum efficiency of QZ1 is 2.5-fold lower than that of asymmetrical ZP4 ($\Phi_{free} = 0.06$)[22b,c] and comparable to that of ZP8 ($\Phi_{free} = 0.03$),[22e] an asymmetrical ZP dye based on 2′,7′-difluorofluorescein. Because of the addition of a second quenching moiety, symmetric QZ2 shows an even more pronounced reduction in background fluorescence, with $\Phi_{free} = 0.005$. This value is comparable to the quantum yields for select benzoate-substituted ZnAF dyes[17k] and represents a ~76-fold reduction in background fluorescence relative to our first Zn(II) responsive dye, ZP1 (Figure 8; Figure S20 displays a comparison of the emission spectra for the Zn(II)-bound sensors).[22a]

In addition to reducing background fluorescence significantly, Zn(II) binding to QZ1 and QZ2 efficiently alleviates PET quenching and restores 75−85% of fluorescein emission (QZ1, $\Phi_{Zn} = 0.78$; QZ2, $\Phi_{Zn} = 0.70$). This behavior greatly contrasts with the turn-on observed for the aniline-derivatized ZP4-type dyes, where fluorescein emission remains substantially quenched following Zn(II) coordination (ZP4 and ZP8, $\Phi_{Zn} \approx 0.3$). Taken together, QZ1 and QZ2 offer significantly enhanced dynamic ranges, ~42- and ~150-fold respectively, as compared to the ZP and ZS sensors previously reported (Table 1) as well as a number of commercially available Zn(II) sensors such as Newport Green.[17i] QZ2 also shows greater fluorescence en-

(33) (a) Jackson, A. P.; Timmerman, M. P.; Bagshaw, C. R.; Ashley, C. C. *FEBS Lett.* **1987**, *216*, 35−39. (b) Kao, J. P.; Tsien, R. Y. *Biophys. J.* **1988**, *53*, 635−639. (c) Quast, U.; Labhardt, A. M.; Doyle, V. M. *Biochem. Biophys. Res. Commun.* **1984**, *123*, 604−611.

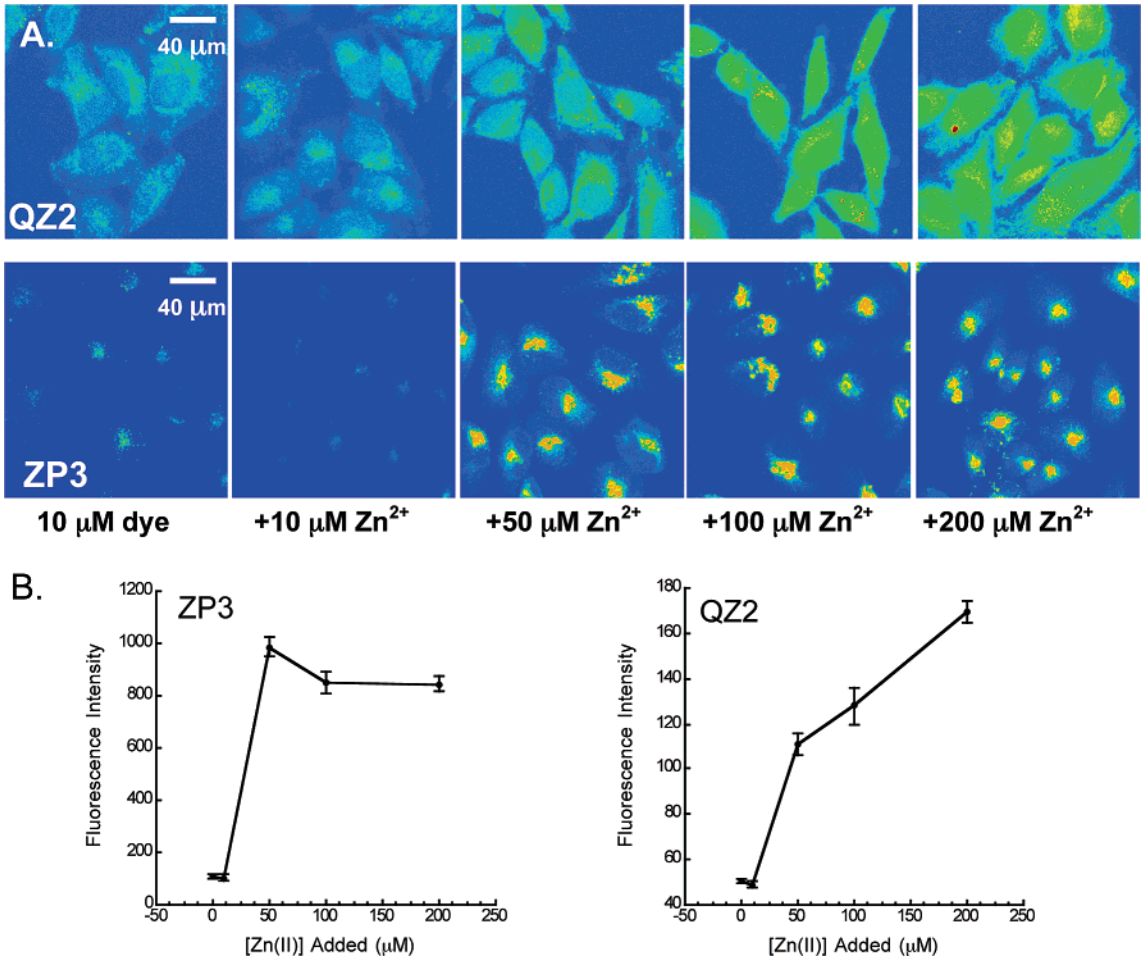

Figure 9. (A) Confocal imaging of fixed HeLa cells treated with QZ2 or ZP3. Top panels: HeLa cells treated with 10 μM QZ2 (4 h, 37 °C) and varying concentrations of Zn(II). Bottom panels: HeLa cells treated with 10 μM ZP3 (30 min, 37 °C) and varying concentrations of Zn(II). The cells were washed once with DMEM containing no FCS before Zn(II) addition and were incubated with Zn(II) for 10 min at 37 °C prior to fixing. A 10:2 Zn(II)/pyrithione ratio was employed. (B) Quantification of the fluorescence response. Left plot: Quantification of ZP3 response. The fluorescence observed in the Golgi was monitored. Right plot: Quantification of QZ2 response. The error bars represent the standard error of the mean (sem) and $p < 0.001$ for the increase observed for QZ2 (Mann−Whitney test). A minimum of 29 cells were quantified at each Zn(II) concentration.

hancement than the benzoate-functionalized ZnAF dyes which, like ZP4−8, suffer from partially quenched fluorescein emission in the Zn(II)-bound forms. Because the fluorescein platform of QZ2 is not halogenated, which lowers the molar absorptivity, the brightness ($\Phi \times \epsilon$) of the Zn(II)-bound species is less than those of ZP1 and ZP3 and similar to that of ZP4 (Figure S19). Incorporation of chloro or fluoro substituents in the 2′- and 7′-positions of the QZ2 fluorophore platform would increase brightness and maintain a QZ2-like dynamic range; however, this modification is unnecessary because QZ2 is readily detectable in vivo (vide infra).

Confocal Imaging and Zn(II) Response in Vivo. Preliminary confocal imaging experiments established that QZ1 and QZ2 are membrane permeable. Given the micromolar K_d value of QZ for Zn(II), we conducted solution studies (50 mM PIPES, 100 mM KCl, pH 7) to determine whether QZ and pyrithione, an ionophore that delivers Zn(II) into cells, compete for Zn(II). Addition of excess 1:2 Zn(II)/pyrithione to QZ resulted in negligible fluorescence change, in agreement with the reported K_d of $\sim 10^{-11}$ M for formation of the 1:2 Zn/pyrithione complex.[34] In vivo experiments were subsequently conducted by treating HeLa cells with 10 μM QZ2 and 100 μM Zn(II) with varying concentrations (0.5−30 μM) of pyrithione. This study indicated that substoichiometric pyrithione delivers Zn(II) into HeLa cells (data not shown, ascertained by fluorescence microscopy), and we therefore employed a 10:2 Zn(II)/pyrithione ratio for all subsequent imaging experiments. Similar results were obtained in a study where the fluorescence response of Zinquin-treated chronic lymphocytic leukemia cells was monitored as a function of varying Zn(II)/pyrithione ratios.[21g] Further control experiments indicated that the Zn(II)-induced fluorescence enhancement of QZ2 is reversible by addition of TPEN to the cell culture medium (Figure S21).

Of particular interest is the use of intracellular Zn(II) sensors with varying K_d values to report on a range of Zn(II) concentrations in cells. To illustrate the utility of a relatively low affinity Zn(II) sensor in vivo, we compared the responses of ZP3 and QZ2 to varying intracellular concentrations of Zn(II). Figure 9 displays HeLa cells treated with 10 μM dye and 0, 50, 100, or 200 μM total Zn(II). ZP3, which has a K_d of 0.7 nM for Zn(II), shows saturation behavior when 50 μM Zn(II) is added to the cell culture medium. In contrast, the fluorescence intensity of cells treated with QZ2, characterized by a micromolar K_d for Zn(II), increases upon addition of up to 200 μM Zn(II). We

(34) Doose, C. A.; Ranke, J.; Stock, F.; Bottin-Weber, U.; Jastorff, B. *Green Chem.* **2004**, *6*, 259−266.

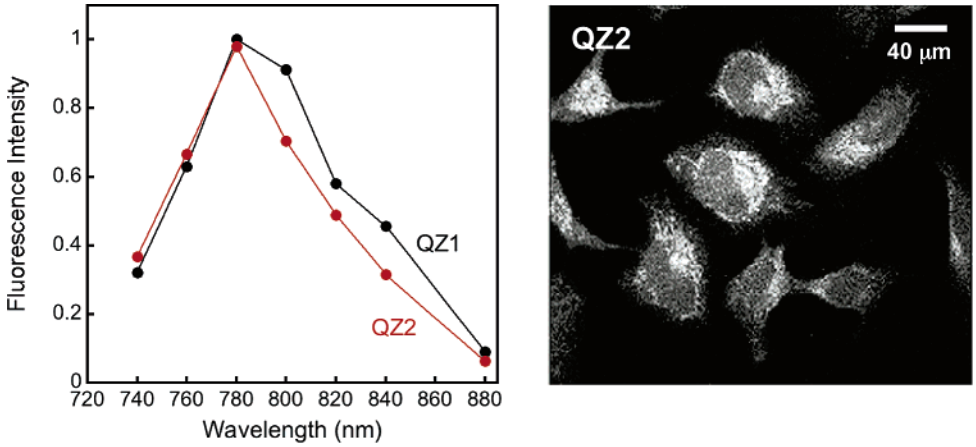

Figure 10. Left: Two-photon excitation profiles for QZ1 (black circles) and QZ2 (red circles) in the presence of 100 μM Zn(II). The solutions were prepared in 50 mM PIPES, 100 mM KCl, pH 7, and [QZ] = 10 μM. The emission was monitored from 0 to 570 nm. Right: TPM imaging of live HeLa cells treated with 10 μM QZ2 (4 h) and 100 μM Zn(II) (5 min, 10:2 Zn(II)/pyrithione, T = 37 °C).

did not exceed this value to avoid Zn(II) toxicity. Although the intracellular concentration of Zn(II) is unclear because sub-stoichiometric pyrithione was used, the results displayed in Figure 9 indicate that probe affinity is an important parameter for in vivo metal ion detection and that lower affinity sensors can be employed to report on relatively high concentrations of the analyte in vivo. This observation is in good agreement with a recent report in which ZnAF sensors with modified DPA ligands showed K_d-dependent Zn(II) responses in vivo[25] and contrasts with a study concluding that relative dye affinity is unimportant for in vivo Zn(II) detection.[35] We note that ZP3 and QZ2 show different staining patterns in HeLa cells, with ZP3 localizing to the Golgi apparatus[22a] and QZ2 showing a more diffuse pattern.

We next investigated ZP3 and QZ2 staining of acute hippocampal slices from adult rat, substructures of which contain histochemically observable zinc. Whereas ZP3 vividly stained the DG and CA3 regions of the hippcampus,[22d] no differential staining was observed following treatment with either QZ1 or QZ2 (Figure S22). This comparison suggests that the levels of endogenous and histochemically observable Zn(II) in the DG and CA3 regions of the rat hippocampus are between the detection limits of ZP3 (K_d < 1 nM) and QZ ($K_d \approx 40$ μM) and further illustrates the utility of Zn(II) sensors with varying dissociation constants for analyzing mobile Zn(II) concentrations in vivo.

Biological Imaging with Two-Photon Microscopy. The development and implementation of new optical imaging techniques parallels advances in chemosensor design. Of recent interest is the application of two-photon microscopy (TPM) to biological Zn(II) imaging.[18c,22e] Optical imaging by TPM offers some advantages over conventional one-photon techniques.[36] By employing two photons of lower energy, laser excitation typically causes less photodamage to dyes and biological samples, and allows for penetration of thicker specimens.

To ascertain the ability of QZ1 and QZ2 to undergo two-photon excitation, the fluorescence intensity of buffered solutions of 10 μM QZ and excess Zn(II) (50 mM PIPES, 100 mM KCl, pH 7) was evaluated following two-photon excitation over the 740−880 nm range. Figure 10 (left panel) displays the relative fluorescence intensity of these solutions and reveals that maximum emission occurs with excitation at 780 nm. Live HeLa cells treated with QZ2 and Zn(II) were imaged by TPM with excitation at 780 nm and are also depicted in Figure 10 (see Figure S23 for a complete set of images), establishing that QZ2 responds to two-photon excitation in vivo.

Summary

The preparation and photophysical characterization of 8-aminoquinline-derivatized, fluorescein-based Zn(II) sensors QZ1 and QZ2 are presented. These dyes have dissociation constants for Zn(II) in the micromolar range, can readily detect Zn(II) in the presence of biologically relevant concentrations of Na(I), K(I), Mg(II), and Ca(II), and display superior selectivity for Zn(II) as compared to other known fluorescent Zn(II) probes. Stopped-flow kinetic analyses show that the QZ dyes display rapid and reversible Zn(II) binding, which affords high temporal resolution and contrasts to the slow dissociation of Zn(II) observed for ZP and other DPA-containing sensors. The results suggest that QZ-type systems will be valuable for biological imaging of Zn(II) flux at elevated concentrations. Because of low background fluorescence and efficient alleviation of PET quenching with Zn(II) coordination, QZ1 and QZ2 afford excellent ~42- and ~150-fold fluorescence enhancement upon Zn(II) binding. A comparison of the photophysical properties of QZ to those of ZP and ZS systems indicates that the nature of the PET switching nitrogen atom is not the only determining factor for fluorescence behavior. Rather, properties of the entire ligand fragment modulate both the degree of fluorescein quenching and the amount of fluorescence turn-on that results from analyte recognition. Quantum calculations will be employed to investigate this matter further. Finally, single-photon and multiphoton microscopy reveal that QZ are cell-permeable and Zn(II)-responsive in vivo. Comparison of the response of QZ2 (micromolar K_d) to that of ZP3 (subnanomolar K_d) to intracellular zinc indicates that sensor binding affinity plays a significant role in metal ion detection in vivo. Efforts to prepare new and utilize current QZ sensors for neurobiological imaging applications are in progress.

(35) Dineley, K. E.; Malaiyandi, L. M.; Reynolds, I. J. *Mol. Pharmacol.* **2002**, *62*, 618−627.
(36) (a) So, P. T. C.; Dong, C. Y.; Masters, B. R.; Berland, K. M. *Annu. Rev. Biomed. Eng.* **2000**, *2*, 399−429. (b) Mainen, Z. F.; Maletic-Savatic, M.; Shi, S. H.; Hayashi, Y.; Malinow, R.; Svoboda, K. *Methods* **1999**, *18*, 231−239. (c) Williams, R. M.; Zipfel, W. R.; Webb, W. W. *Curr. Opin. Chem. Biol.* **2001**, *5*, 603−608.

Acknowledgment. This work was supported by Grant GM65519 from the National Institute of General Medical Sciences. Spectroscopic instrumentation at the MIT DCIF is maintained with funding from NIH Grant 1S10RR-13886-01 and NSF Grants CH3-9808063, DBI9729592, and CHE-9808061. M.S. is an Investigator at the Howard Hughes Medical Institute. E.M.N. thanks NDSEG for a graduate fellowship, Drs. C. J. Chang and D. Xu for insightful discussions, and Dr. L. G. Beauvais for assistance with the stopped-flow experiments.

Supporting Information Available: Full listing of authors of ref 14; Figures S1−S23, which include fluorescence titrations (S1); the reversibility of QZ binding to Zn(II) following TPEN addition (S2); a Job plot for Zn(II) binding to QZ1 (S3); metal ion selectivity plots for QZ1 (S4); representative kinetic traces and plots of k_{obs} versus initial [dye] (S5−S9); plots of k_{obs} versus [Zn(II)] (S10−S14); Eyring plots (S15−S19); relative fluorescence emission of the Zn(II)-bound sensors (S20); and both confocal and two-photon microscopy images of biological samples (S21−S23); and experimental details for the representative kinetic analyses. This material is available free of charge via the Internet at http://pubs.acs.org.

JA052184T